A Contoured-Beam Reflector Satellite Antenna Using Two Doubly Curved Circular Polarization Selective Surfaces

Andreas Ericsson, *Member, IEEE*, Daniel Sjöberg, *Senior Member, IEEE*,
Giampiero Gerini, *Senior Member, IEEE*, Cecilia Cappellin, *Member, IEEE*,
Frank Jensen, *Life Member, IEEE*, Peter Balling, Life *Member, IEEE*,
Nelson J. G. Fonseca, *Senior Member, IEEE*,
and Peter de Maagt, *Fellow, IEEE*

***Abstract*—We present a reflector antenna system using a circular polarization selective surface (CPSS) to realize a circular polarization (CP) equivalent to the widely used linear polarization (LP) gridded or dual-gridded reflector (DGR). The CPSS is realized by a multilayer stack of non-resonant anisotropic meander line surfaces, achieving a very wide bandwidth. The CPSS reflection and transmission dyadics are computed using full-wave simulations for all angles of incidence and design frequencies applicable, and the doubly curved reflector surface shapes are optimized in the TICRA POS software. The data are input to the TICRA Tools software framework for antenna-system level radio frequency (RF) simulations. A planar CPSS sample was first manufactured and tested to demonstrate the adequacy of the selected multilayer design. A doubly curved reflector demonstrator based on the same technology and with a projected aperture of 750 mm was then designed, manufactured, and tested at Ku-band. While promising, the experimental results emphasize the difficulty of producing an electrically large multilayer doubly curved surface with RF performance equivalent to the original flat design and recommendations are provided to improve further the implementation of the proposed design.**

***Index Terms*—Circular polarization (CP), circular polarization selective surface (CPSS), doubly curved demonstrator, polarization selectivity, reflector antenna**

I. INTRODUCTION

TODAY a high number (few hundreds) of large communication satellites, mainly located along the crowded geostationary (GEO) orbit, provide direct broadcast services, Internet services and a multitude of other important fixed and mobile communication services. There is clearly a need for higher payload integration and multi-mission spacecrafts where accommodation of multiple large reflector antennas is often the limiting factor. One option would be to have a multi-frequency antenna system, such as a shaped reflector covering multiple bands of interest, e.g. C and Ku-band. But this leads to mission specific equipment and trade-offs, whereas the idea pursued in this paper is to simplify the antenna farm for a given frequency band independently of the other antenna farms embarked at other frequency bands.

Very efficient GEO satellite antenna systems have been developed for direct broadcast services (DBS) based upon gridded or dual-gridded reflector (DGR) antenna configurations for linear polarization (LP) with a shaped reflector surface, or shell, illuminated by a high power feed in the focal plane of the appropriate polarization [1, pp. 282-285, 488-489, 710], [2, pp. 32-39]. Dual-gridded reflector antenna configurations combined with small passive arrays are also reported for satellite communication ranging typically from C to Ku-band [3]-[8], with a few developments also reported at Ka-band [9], [10]. Usually, the LP DGR front shell is gridded to reduce the offset-reflector cross-polarization while the rear shell is solid to improve the stiffness. Configurations using gridded sub-reflectors have also been investigated for multiple contoured beam applications [10]-[12]. These configurations combine the functionalities of two reflectors, operating over the same frequency band, e.g. Ku-band, in the physical aperture of one and provide high cross-polarization discrimination (XPD) and both low feed system and spillover losses. There is some interest in extending this technology to higher frequency bands, including Direct Broadcast Satellite (DBS) frequencies in the upper range of the Ku-band, where signals are predominantly circularly polarized (CP) to avoid polarization alignment and facilitate terminal installation, thus requiring a CP equivalent to the LP DGR.

In recent times, dual reflectors of the Gregorian or Newtonian type have been used more often than DGR's, as they have reduced complexity, reduced interaction between the reflectors and improved out-of-coverage performance to name of a few of their advantages. However, dual reflector configurations with small sub-reflectors are also known to

Manuscript received February 8, 2019. Date of publication September 30, 2020. This work was supported by the European Space Agency (ESA) in the frame of the Technology Research Programme (TRP) under Contract 4000108854/13/NL. (Corresponding author: Andreas Ericsson.)

Andreas Ericsson, Cecilia Cappellin, and Frank Jensen are with TICRA, DK-1119 Copenhagen, Denmark (e-mail: ae@ticra.com; cc@ticra.com; fj@ticra.com).

Daniel Sjöberg is with the Department of Electrical and Information Technology, Lund University, 221 00 Lund, Sweden (e-mail: daniel.sjoberg@eit.lth.se).

Giampiero Gerini is with the Optics Department, TNO, 2628 CK Delft, The Netherlands, and also with the Electromagnetics Group, Eindhoven University of Technology, 5212 AP Eindhoven, The Netherlands (e-mail: giampiero.gerini@tno.nl).

Peter Balling is with ASC, DK-2600 Taastrup, Denmark (e-mail: pballing@asc-consult.dk).

Nelson J. G. Fonseca and Peter de Maagt are with the Antenna and Sub-Millimetre Wave Section, European Space Agency (ESA), 2200 AG Noordwijk, The Netherlands (e-mail: nelson.fonseca@esa.int; peter.de.maagt@esa.int).

suffer from significant scan aberrations. Current missions tend to have wide service areas, sometimes even global coverage. Hence, a CP equivalent to the LP DGR antenna is of high interest.

A number of CP antenna configurations equivalent to the LP DGR were investigated by a large pan-European team [13]. Promising solutions, based on transmission CP polarizers, were identified and the well-known meander line polarizer was preferred for its potential for wide or dual-band operation, low axial ratio (AR), and low insertion loss (IL). However, no experimental demonstration was implemented in the frame of that study as no solution proved to be sufficiently competitive both commercially and with respect to radio frequency (RF) performance. Circular polarization selective surface (CPSS) solutions were not addressed in the frame of the study as those solutions seemed to lack maturity and had rather limited operating bandwidth resulting from the use of resonant wire cranks [14]-[16] or coupled resonant elements [17]-[18], although in principle they could lead to simpler antenna configurations fully equivalent to the above mentioned LP DGR.

In recent years, significant advances have been reported in designing CPSS with wider bandwidth and improved RF performance at oblique incidence angles compared to previously reported CPSS designs [19]-[27]. A key component in this improvement is the fact that anisotropic sheets have been utilized to construct the CPSS in place of resonant wire elements. In [19]-[20], a wideband CPSS was realized by cascading two meander line polarizers, converting LP to CP and vice versa, with a strip grid layer in between the polarizers. These structures achieve a relative bandwidth of about 26% but require seven layers and have a total thickness of about $1.5\lambda_0$, where λ_0 is the wavelength in free space. A similar but improved design was presented in [25]-[26] where a CPSS is realized by cascading meander line sheets with a relative rotation of each layer, resulting in a relative bandwidth of 56% with respect to the same requirements as was used in [19], [20]. This solution is considered of interest for space applications as lower insertion losses are anticipated when compared to the previously studied solutions combining LP-to-CP polarizers and a strip grid layer. The meander lines may be DC grounded along the polarizer rim for electrostatic discharge (ESD) mitigation as in LP DGR's. Preliminary analyses have been reported in [22]-[25]. In this paper, a practical implementation of this multilayer CPSS concept is proposed for Ku-band using materials that are qualified for space applications and compatible with manufacturing processes enabling molded doubly curved surfaces. To the best of the authors' knowledge, this is the first time that an electrically large doubly curved CPSS demonstrator is manufactured and tested. The paper is organized as follows; In Section II.A dual CPSS reflector antenna system is presented, and a proposed CPSS design is introduced. Additionally, a suggested application of the system is described and simulated. In Section III relevant fabrication methods are discussed and the fabrication and testing of a flat CPSS demonstrator, as well as a doubly curved CPSS demonstrator, are presented. Finally, some concluding remarks are put forward in Section IV.

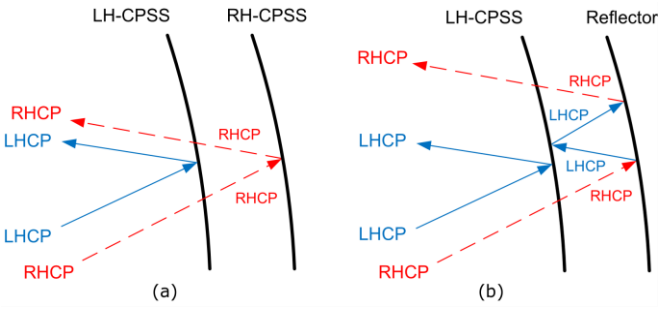

Fig. 1. Dual-CPSS geometries equivalent to DGR in CP: in (a) two reciprocal and symmetric CPSS of orthogonal selectivity are combined and in (b) the combination of an LH-CPSS and a solid reflector is presented.

II. Dual Reflector Antenna System

A. Contoured Beam Mission and Antenna Requirements

The targeted mission scenario consists of a Ku-band fixed-satellite service (FSS) contoured-beam with Australian coverage. This specific application is selected to demonstrate the capability of the proposed CPSS technology to cover a wide fractional bandwidth. A CP-equivalent of a dual gridded reflector system is proposed, where two shaped CPSS reflectors are sharing a single aperture. The front reflector is a reciprocal symmetric left hand CPSS (LH-CPSS) that reflects LHCP and transmits RHCP. The back reflector is a reciprocal symmetric right hand CPSS (RH-CPSS) that reflects RHCP and transmits LHCP, as is illustrated in Fig. 1 (a). The polarization state is maintained in both reflection and transmission from both reflectors since they are reciprocal symmetric CPSSs.

The rationale behind the use of a CPSS for the rear shell, rather than a solid reflector as usually done in LP DGR antenna systems, is to avoid multiple reflections between the two shells for the polarization reflected by the rear shell, as can be seen in Fig. 1 (b). In addition, the proposed multilayer CPSS design has enhanced stiffness when compared to a gridded reflector.

The dual reflector antenna system operates at the frequencies 10.70-12.75 GHz in transmit (Tx) and 12.75-14.50 GHz in receive (Rx), corresponding to a fractional frequency bandwidth of about 30%. For applications requiring a wider bandwidth, such as DBS services, a dual-band CPSS design [27] would be more suitable. However, this would require more layers in the CPSS stack-up, which would be a real challenge for antenna designs requiring doubly curved CPSSs as it will be fully evidenced in this paper. System analyses for the specific mission were carried out to derive the antenna requirements to be targeted. It was concluded that a minimum directivity of 29.0 dB is suitable from a link budget perspective and the XPD should be larger than 25 dB. The geometrical parameters of the reflector system were specified based on these antenna requirements, and it was proposed to use parabolic reflectors with a circular rim of 1.0 m diameter. The feed displacement was chosen to be 0.6 m from the axis of the parabolic antenna. The

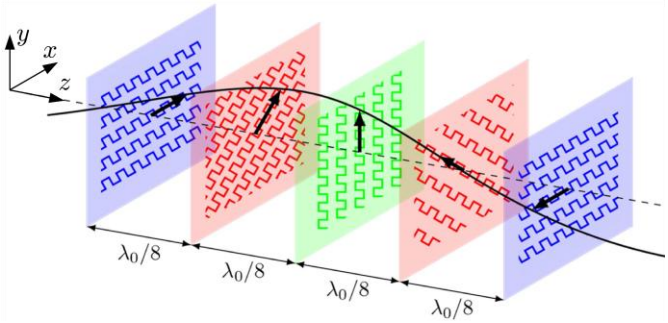

Fig. 2. Concept design of the CPSS. The electric field of an LHCP wave has been indicated at each sheet to illustrate the operating principle.

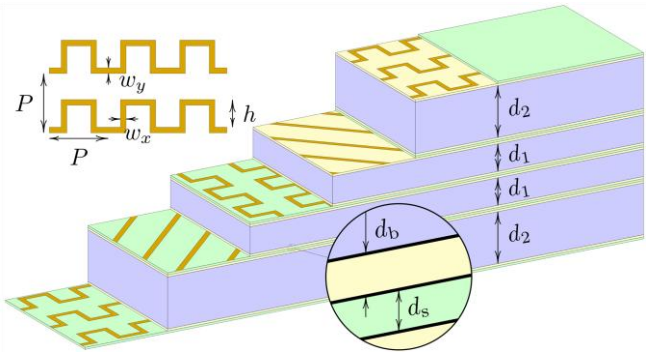

Fig. 3. Definition of the geometrical parameters of a five-layer CPSS.

parabolic surfaces have a focal length of 1.1 m and 1.0 m for the back and front surface, respectively. Gaussian beams with a taper of -12 dB at the edge of the reflectors are used to model the feeds. It was further specified that the CPSS surfaces should fulfil the unit cell requirements of return loss (RL) and IL lower than 0.5 dB. The XPD should be better than 27 dB for small incidence angles, corresponding to AR lower than 0.78 dB.

B. CPSS Multilayer Design

The CPSS developed in this work utilizes the concept presented in [25]-[27]. It is based on cascaded non-resonant anisotropic layers realized as printed circuit boards with meander line patterns as in Fig. 2. The concept of operation of the structure is based on rotating the subsequent layers at the same rate as the wavelength of the incident CP wave, as is illustrated in Fig. 2, following the principle of screw-symmetry [28], also referred to as twist-symmetry in optical systems. The circular polarization that aligns with the layers will be reflected and the orthogonal polarization is transmitted. To this end, each consecutive layer is rotated 45° and the spacing between the sheets is about $\lambda_0/8$ where λ_0 is the free space wavelength at the center frequency of the operating bandwidth. The period of the structure in each layer is on the order of $\lambda_0/4$, which implies desirable stability with respect to angle of incidence variations. In the final design, the sheet separation and the meander line parameters are optimized using full-wave simulations. The geometrical parameters of the CPSS are defined in Fig. 3.

TABLE I
MATERIAL PARAMETERS OF THE CPSS

MATERIAL	PERMITTIVITY	Loss tangent	Thickness
Spacers	1.10	0.0020	d_1 and d_2
Substrates	2.62	0.0114	d_s
Bond films	2.77	0.0050	d_b
Metal lines	Copper, σ = 5.6e7 S/m		18 μm

TABLE II
GEOMETRICAL PARAMETERS OF THE CPSS

Meander line parameters				Multilayer parameters	
P	5.28	h_1	0.00	d_1	2.61
w_{0x}	0.51	w_{2y}	0.16	d_2	4.91
w_{0y}	0.58	w_{2x}	0.17	d_s	0.10
h_0	2.46	h_2	2.43	d_b	0.05
$w_{1x/y}$	0.12				

All dimensions are in mm.
For the meander line parameters, index 0 refers to the middle layer, index 1 to the next layers and index 2 to the outmost layers.

The CPSS was designed to fulfil the requirements introduced in Section II.A. Those requirements being quite challenging, it was agreed to provide the best possible performance in line with the requirements for incidence angles corresponding to the central part of the reflector, where most of the RF power is impinging. Slightly degraded performance was considered acceptable for angles of incidence corresponding to the outer rim of the reflector where less RF power will be impinging. It was thus decided that the CPSS XPD should be at least 20 dB for incidence angles larger than 25° corresponding to AR < 1.75 dB.

When implementing a CPSS in an offset antenna system, the structure will operate at oblique angles of incidence. This implies that the relative orientation of the CPSS with respect to the feed is of significant importance. In [25], the performance of a meander line CPSS was evaluated for all angles of incidence at a few discrete frequencies, and it was concluded that the optimum performance for such a structure is achieved in the incidence planes $\phi = (2n\text{-}1)\times 45°$, n = 1,2,3,4. Due to the symmetry of the structure, the reflection and transmission properties of the CPSS are symmetric with respect to θ [25]. To this end, the CPSS in this work is oriented at the azimuth angle $\phi = 45°$ with respect to the feed antenna. The relative orientation of the CPSS is given in Fig. 2, and a conventional spherical coordinate system was used to define the incidence angles θ and ϕ in relation to the Cartesian coordinates, see [29] for further details.

The frequency domain solver of Computer System Technology Microwave Studio (CST-MWS) was used to optimize the CPSS with the design scheme presented in detail in [26]. The CPSS was modeled as a periodic structure of infinite extent in the plane orthogonal to the normal vector of the panel, and the design parameters w_{ij}, h_i, d_k and P were used as optimization parameters, where i = 0,1,2, j = x,y and k = 1,2. The Material characteristics used in the simulation model are listed in Table I, and the final geometrical

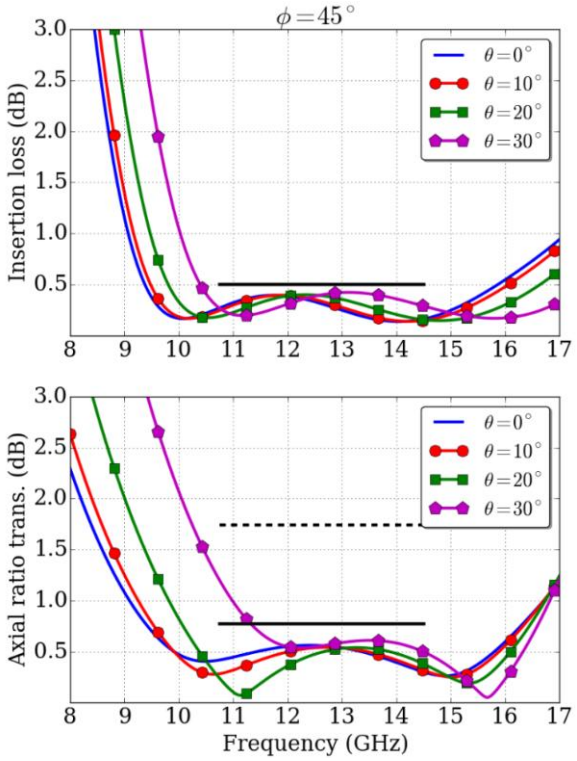

Fig. 4. Simulated transmission of the multilayer meander line CPSS. The bold black lines represent the design requirements, and the dashed black lines are the relaxed design requirements for the AR. The plane of incidence is $\phi = 45°$.

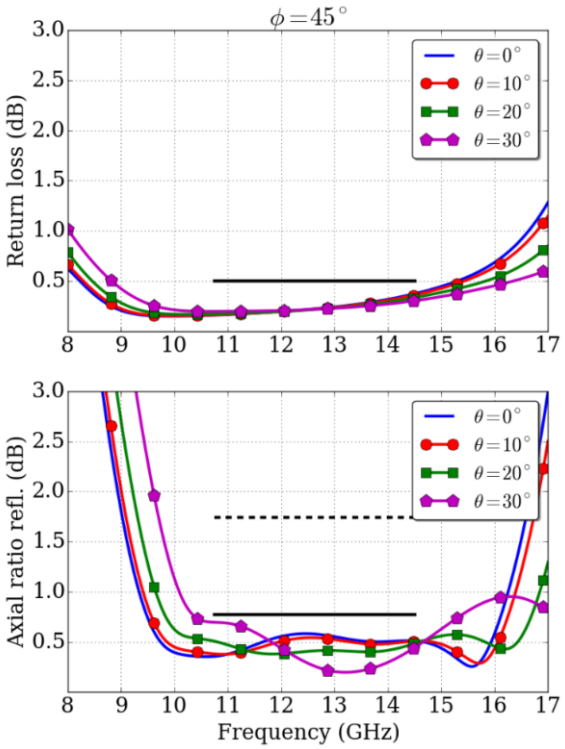

Fig. 5. Simulated reflection of the multilayer meander line CPSS. The bold black lines represent the design requirements, and the dashed black lines are the relaxed design requirements for the AR. The plane of incidence is $\phi = 45°$.

parameters following the optimization process described in [25] are reported in Table II. The choice of materials and associated fabrication processes are further detailed in Section III.

When a design with desirable performance had been achieved, the scattering of the optimized design was simulated using a finer mesh setting to verify convergence. Numerical results of the optimized CPSS design are reported in Fig. 4 and Fig. 5 for transmission and reflection, respectively. Here it can be seen that the requirements of RL and IL lower than 0.5 dB are fulfilled for the incidence angles $\theta = [0,30]°$, and that the strict requirement of AR < 0.78 dB is fulfilled for $\theta = [0,20]°$, while the relaxed requirement of AR < 1.75 dB is fulfilled for $\theta = [0,30]°$.

C. *Antenna System Analyses*

The antenna system introduced in Section II.A was implemented and simulated in TICRA Tools as a dual-CPSS reflector, where the front reflector is a reciprocal symmetric LH-CPSS and the back reflector is a reciprocal symmetric RH-CPSS [24], as can be seen in Fig. 6. Ideally, the field of an LHCP feed (the front shell feed) will be reflected by the front reflector to an LHCP far-field, and the field of an RHCP feed (the back shell feed) will be transmitted by the front reflector and will be reflected by the rear reflector to an RHCP far-field, which again will pass through the front reflector to the far-field. The reflectors were shaped at 12 GHz, using the TICRA software POS, to an Australian coverage from a geostationary satellite at 130° East, resulting in the surfaces in Fig. 6. The design goal in the shaping of the reflectors was specified such that an XPD of at least 27 dB

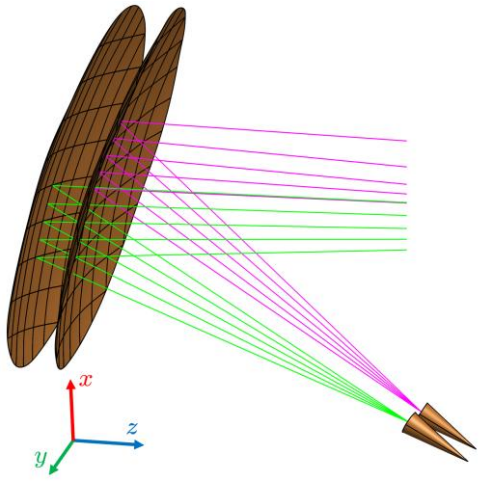

Fig. 6. Dual-CPSS reflector simulated in TICRA Tools. The rays from the LHCP feed (pink) are reflected by the front reflector and the rays from the RHCP feed (green) are reflected by the back reflector.

should be achieved. This requirement is equivalent to the AR requirement, which was specified for the CPSS unit cell design.

Two different scenarios were simulated; First the dual reflector surfaces were represented by ideal CPSSs (with zero dB IL, RL and AR), and then the reflectors were represented by the scattering properties of the CPSS design proposed in Section II.B. In the second case, the CPSSs were simulated in TICRA Tools using a .tep file as input in which the transmission and reflection properties of the surface are given in a rectangular grid of the oblique angle of incidence θ and the azimuth angle ϕ. These reflection and transmission coefficients of the unit cell CPSS design were computed

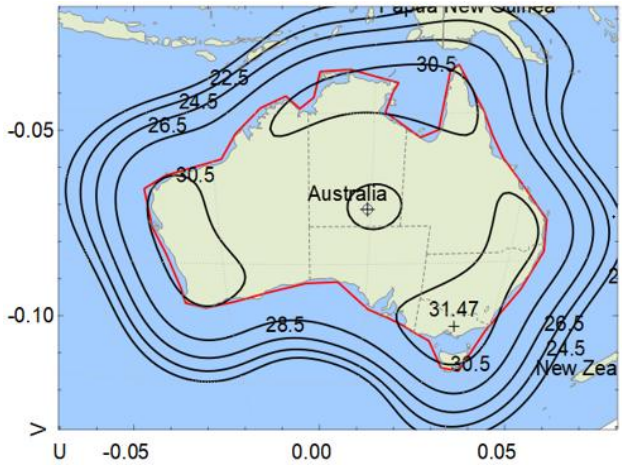

Fig. 7. LHCP coverage of an ideal CPSS reflector antenna pattern in dBi at 12.625 GHz. The LHCP front shell feed is illuminating the reflector consisting of an ideal LH-CPSS.

using CST-MWS for both polarizations and all angles of incidence from both sides of the structure, using a discretization of 5° in θ and ϕ. The data were then transformed from .s4p (Touchstone) into the .tep-format used in TICRA Tools.

The antenna radiation from the whole system was calculated using physical optics (PO). To account for the coupling between the front and the back reflector, the PO solver was used iteratively together with a plane wave expansion (PWE). This way, the currents induced on the front reflector by the rear reflector, and vice versa, were determined up to the second order. The antenna system results in Section II.C correspond to the total scattered field from both the front and the rear reflector, in both the co-polar and cross-polar component. The antenna contour results were finally exported from TICRA Tools and imported into SATSOFT for its enhanced visualization functionalities.

For the reflector system with ideal CPSSs, the minimum co-polar gain within the coverage region is 29.4 dBi for the RHCP beam and 29.3 dBi for the LHCP beam, at the center frequency 12.625 GHz. The LHCP antenna system coverage from the LHCP feed illumination is presented in Fig. 7, where contour levels are marked in black and the values are in dB. A map over the Australian region can be seen and the coverage within which the field was evaluated is marked in red. Since ideal CPSSs were used in this simulation the cross-polar fields are negligible (XPD > 60 dB) and are thus not presented. It was observed that the co-polar gain was reduced at the outer frequencies of the band of operation. At the lowest frequency, the gain was reduced by 0.8 dB for both beams, and at the highest frequency the gain was reduced by 2.3 dB for both beams.

The second simulation case with the shaped, realistic CPSSs, was investigated in multiple iterations. Here the unit cell scattering parameters of the CPSS design in Section II.B were imported using different orientations of the azimuth angle of the CPSS in the global antenna coordinate system. The *x*-, *y*- and *z*-axis of the global coordinate system is given by red, green and blue arrows, in Fig. 6 and the antenna system is offset in the *x*-direction. It was concluded that orienting the CPSSs at an azimuthal angle of $\phi = 45°$ resulted

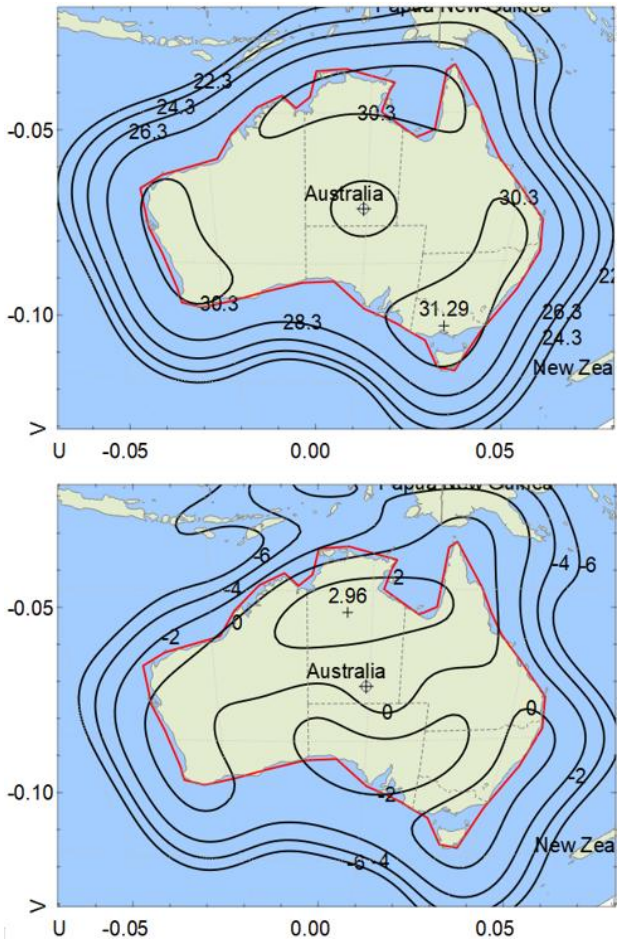

Fig. 8. Co-polar LHCP coverage (top) and cross-polar RHCP coverage (bottom) of a realistic LH-CPSS reflector antenna system at 12.625 GHz. The reflector is illuminated by an LHCP feed.

in the best cross-polar performance of the antenna system, which is equivalent to minimizing the coupling between the two surfaces. This conclusion is in line with the oblique incidence scattering results of a similar CPSS presented in [25]. The co-polar and cross-polar patterns for LHCP (front shell feed) illumination at 12.625 GHz are presented in Fig. 8 for the described CPSS orientation. The cross-polar levels of the antenna pattern are ranging between -3.81 dBi and 2.96 dBi, within the coverage region, and the co-polar coverage pattern is between 29.19 dBi and 31.29 dBi. These results correspond to a worst-case XPD of 26.44 dB within the coverage region. At the outer frequencies of 10.75 GHz and 14.5 GHz, the co-polar gain is reduced by about 0.8 dB in relation to the peak gain at the center frequency, and the XPD at the outer frequencies are 25.5 dB and 30.0 dB, respectively.

For RHCP (back shell feed) illumination, the cross-polar levels of the antenna pattern are between -3.95 dBi and 2.61 dBi, and the co-polar pattern is between 28.71 dBi and 30.78 dBi, at the center frequency. This corresponds to a minimum XPD of 26.1 dB in the full coverage region. At both the highest and lowest frequency the coverage gain is reduced by 2.7 dB in relation to the center frequency, and the corresponding XPDs are 28.6 dB and 29.0 dB, respectively.

When comparing the results of the LHCP (front shell feed) and the RHCP (back shell feed) illumination it is noted that the co-polar performance of the two coverage beams is comparable. The difference in co-polar gain between the ideal CPSS reflector system and the realistic system is 0.2 dB for LHCP illumination and 1.1 dB for RHCP illumination. The RHCP co-polar coverage suffers from larger gain loss at the outer frequencies, but in return provides higher XPD than the LHCP beam. The XPD of the antenna system is better than 25.5 dB over the full coverage region for the specified frequency range, and the co-polar gain inside the coverage region is better than 28.4 dBi for LHCP illumination and 26.0 dBi for RHCP illumination.

In order to investigate the magnitude of the coupling between the two surfaces, the scattered field was extracted for the LHCP beam and the RHCP beam with and without the CPSS reflector of orthogonal handedness present. It was found that for RHCP illumination the co-polar coverage is reduced by 0.5 dB, and the corresponding XPD is reduced by 1.5 dB, due to the introduction of the LH-CPSS reflector in front of the RH-CPSS reflector. In the case of LHCP illumination, both the co-polar coverage and the XPD are basically unaffected by the introduction of the RH-CPSS reflector behind the LH-CPSS reflector. Furthermore, in Fig. 8 the peak of the cross-polar pattern occurs inside the targeted co-polar region. This is caused by cross-polar reflection from the LH-CPSS and can thus not be compensated for by shaping the surface or re-orienting the feeds.

III. Hardware Manufacturing and Testing

A. Planar CPSS Sample

To secure the manufacturing of the doubly curved CPSS demonstrator, a planar CPSS sample was first manufactured and tested to validate the choice of materials. The materials and manufacturing process were discussed in parallel of the detailed design of the CPSS, reported in Section II.B, enabling to take into account early in the design phase constraints coming from available materials. The trade-off on materials was mainly driven by manufacturability, stiffness, and weight considerations compatible with the mission scenario described in Section II.A.

Based on the heritage from previous studies [13], a combination of space qualified materials with the required properties have been identified, which consists of:

1) Layers of Kapton foils as support for a copper clad, which can be etched (e.g. laser or photo etching) to get the required meander lines with the required line width and geometry.
2) Local stiffeners providing the required stiffness for each electrical layer, consisting of Kevlar/Cyanate Ester composite. This composite has good thermal properties. Having a negative fiber Coefficient of Thermal Expansion (CTE), one can achieve a near zero CTE composite and the total electrical layer CTE can be kept low as well. For Kevlar fibers, high moisture uptake must be taken into account. RF properties are still acceptable for this composite.

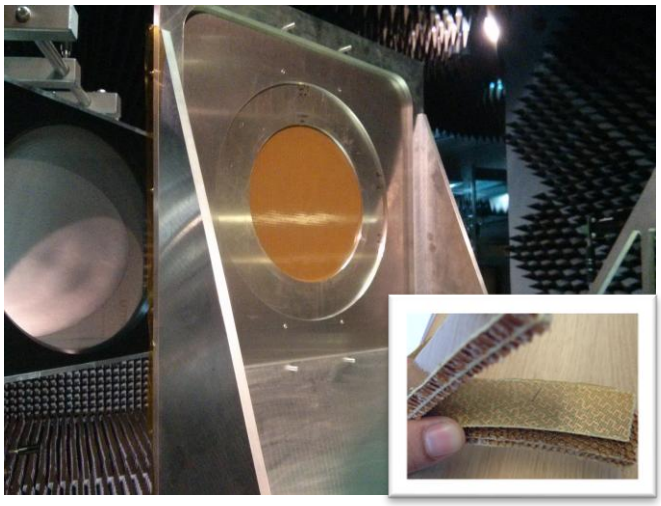

Fig. 9. Flat CPSS panel demonstrator mounted in its support frame for testing purposes. Bottom right inset: image of a disassembled cut-out of the demonstrator panel.

3) Spacers, which may be one of the following three materials: aramid honeycomb core (e.g. Nomex, Kevlar), Rohacell foam core or Quartz honeycomb core. These three materials are all good dielectrics. Quartz honeycomb and Rohacell have the least loss factors. Honeycombs are orthotropic both mechanically and RF-wise, while Rohacell can be considered isotropic. Nomex honeycomb was finally chosen for the demonstrator.

A picture of the flat sample demonstrator, mounted on its supporting frame for testing purposes, is provided in Fig. 9, including a detailed view of a multilayer cut-out which was disassembled for inspection purposes. The planar CPSS sample, with dimensions 300 mm x 300 mm, was tested using the Material RF Characterization Free-Space Test Facility available at the European Space Research and Technology Centre (ESTEC) of the European Space Agency, The Netherlands. Two test configurations are visible in Fig. 10 (a) and 10 (b), corresponding to a test in transmission and a test in reflection, respectively. This free-space quasi-optical system, operating from 8 GHz up to 110 GHz, enables high-purity LP operation (with an XPD better than 50 dB) thanks to the use of wire-grid polarizers in front of the two feed blocks, each of them being composed of a corrugated horn and an offset parabolic reflector antenna.

The feed blocks, operating in transmit and/or receive depending on whether the sample under test is characterized in transmission or reflection, produce a plane wave with a beam-waist diameter of about 5 wavelengths at the lowest frequency of operation of the measurement system, thus minimizing the interference with the sample holder and surrounding items. The use of a wire-grid prevents the measurement of the coupling between E and H modes in reflection. Thus, performance in reflection at normal incidence cannot be measured. The minimum angle of incidence measured in reflection is 20°, due to the large dimensions of the feed blocks, as visible in Fig. 10 (b).

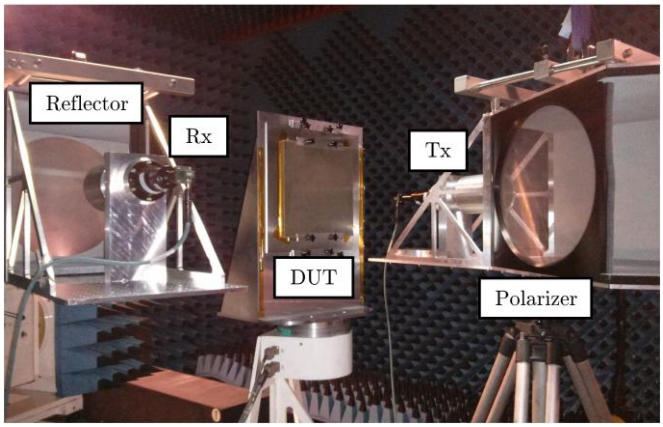

(a)

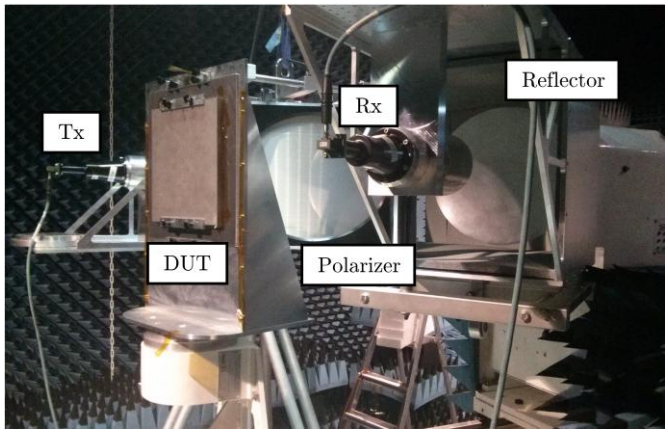

(b)

Fig. 10. Flat CPSS panel demonstrator in two different experimental configurations for (a) transmission scattering measurements and (b) reflection scattering measurements.

As the feed blocks operate in linear polarization, post-processing is applied to convert LP into CP field components. The transmitting and receiving feed blocks were arranged in horizontal (H) or vertical (V) orientation and all four combinations HH,VV,HV,VH were evaluated. This process was carried out first for the device under test (DUT) and later for a reference case used for normalization. In the transmission case, reference measurements were carried out with the DUT removed, and in the reflection case the DUT was replaced by an aluminium panel.

Experimental results of the planar CPSS demonstrator are presented in Figs. 11-12, where the transmission and reflection properties of the DUT are presented for different oblique angles of incidence θ. The performance of the CPSS was evaluated in different incidence planes given by $\phi_n = (n\text{-}1)\times 45°$, where n = 1,2,3,4. The incidence plane ϕ_1 = 0° corresponds to illuminating the CPSS at angles parallel to the outer meander lines of the cascade, and the incidence plane ϕ_2 = 45° corresponds to an azimuthal rotation with respect to the outer meander line layers.

Good agreement is achieved between simulations and experimental results, both in transmission and reflection, for the different combinations of the incidence angles θ, ϕ. The IL in Fig. 11 fulfills the specified requirement at normal

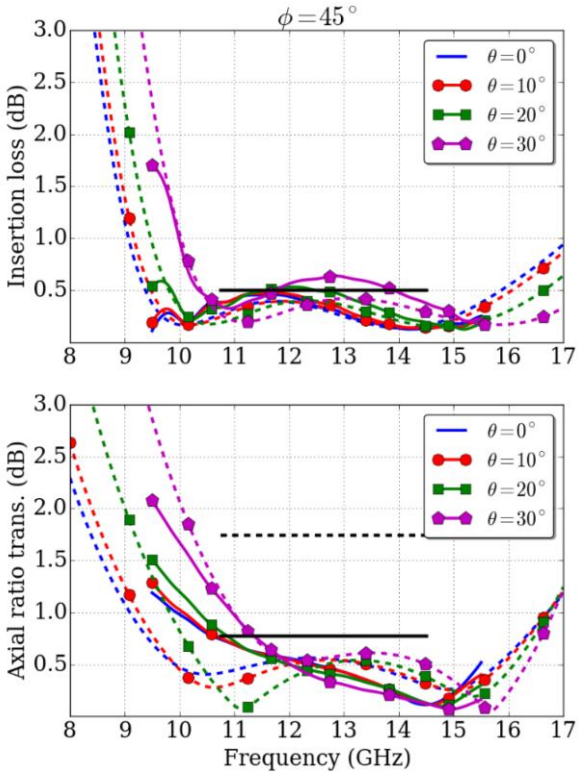

Fig. 11. Transmission results of a fabricated planar CPSS demonstrator, where experimental results are given by solid curves and simulations are given by dashed curves. The measurements were carried out at the incidence angles θ = 0,10,20,30° in the incidence plane ϕ = 45°.

incidence and at larger oblique angles of incidence the experimental results are slightly higher than the corresponding simulations. The RL in Fig. 12 just about fulfills the specified requirements. It can be seen that the RL curves are below 0 dB for some frequencies. This result is unphysical and is likely caused by small misalignments, or differences in curvature, between the DUT and the reference panel in the subsequent reflection measurements. An experimental method was recently presented in [26] where this problem is avoided by using a thin aluminum film rather than a separate panel for reference measurements in reflection. This alternative method could be of interest for future investigations.

The deviation between simulations and experimental results are slightly larger in AR than in IL and RL, which is in-line with what has previously been presented in [25]-[27]. This is likely due to small variations in the measurement setup between subsequent measurements, small antenna/test panel misalignments, or small imperfections in the fabricated demonstrator, which can result in noticeable variations in the polarization purity of waves scattered by the CPSS. However, the measured AR curves in Figs. 11-12 are at desirable levels and only significantly passes above the requirement levels at larger oblique angles of incidence in reflection.

When comparing the results in Figs. 11-12 versus the results achieved for the other incidence planes that were considered, it was noted that the CPSS performs best in the incidence planes ϕ = 45° and ϕ = 135°. This effect was previously anticipated through simulations of a similar CPSS

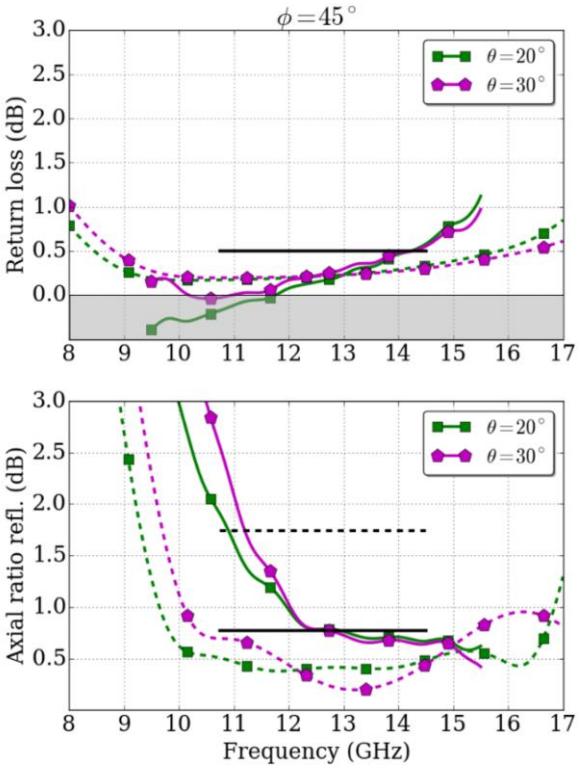

Fig. 12. Reflection results of a fabricated planar CPSS demonstrator, where experimental results are given by the solid curves and simulations are given by dashed curves. The measurements were carried out at the incidence angles θ = 20,30° in the incidence plane ϕ = 45°.

in [25], but the results in Figs. 11-12 provide the first experimental verification of the fact that such a CPSS has preferred incidence planes of operation.

B. Doubly Curved CPSS

For the purpose of demonstration, a doubly curved (centered paraboloid) CPSS reflector with a projected diameter D = 75 cm and a focal length f = 75 cm (f/D = 1) was selected to be representative of the expected surface curvature in a typical mission like the one described in Section II.A. From a manufacturing point of view, two main challenges are faced. First, the deposition of metallic patterns on multilayer and doubly curved surfaces. Second, the necessity to handle a relatively large curved structure. Unfortunately, at the time of the project execution (but the following statement is still essentially valid today), there were no easily available/standard manufacturing technologies for the production of large doubly curved multilayer metal-dielectric structures. In the framework of the project, a proper assessment study of different non-conventional manufacturing technologies was performed, in order to identify the best approach for the realization of a representative demonstrator. The trade-off to select the required manufacturing approach was driven by the following main criteria:

- maturity of the technology;
- costs;
- capability to handle large surfaces;
- capability to work with space qualified materials.

Two main techniques were envisaged and are further detailed in the following two sections.

1) Deposition of Metallic Traces Directly on Doubly Curved Supports

This approach relies on metal deposition techniques such as Laser Direct Structuring (LDS) or active ink-jet printing. The main issues, in this case, are the maximum size of the area to be treated and the availability of manufacturing instrumentation capable to work with non-planar surfaces with the desired dimensions. Active ink-jet printing did not represent a viable solution based on those issues.

With LDS, the metallic patterns can be directly translated from CAD drawings to the surface. The process consists of three steps: 1) First molding a component from thermoplastic resin doped with an organometallic material; 2) Circuit layouts are patterned on the molded component using a laser beam to create the desired circuit paths; 3) The laser defined pattern is then plated with electroless copper. LDS can be used directly on curved surfaces, but the existing tools allow handling only objects of maximum size 35-40 cm. This would have required to decompose the structure in several small parts to be properly reassembled. For this reason, this approach has not been considered as the preferred option.

2) Conventional Etching on Flat Thin Films

This approach poses no challenges for the etching process, which can be performed resorting to conventional technologies applied to thin dielectric films. The main challenges are in the application of these thin films, with the metallic traces, on doubly curved dielectric supports. This is a particularly delicate phase which can hamper the quality of the whole demonstrator. It is clear in fact, from geometrical considerations, that during the process there will be a creeping of the flat surface which needs to be controlled by using the elasticity of the film. It is also clear that this will produce some deformation of the original meander line geometry, which is difficult to anticipate by design.

The overall process consists of the following six steps:

1) Build mold tool;
2) Produce photo-tools;
3) Print and etch flexible tracking layers;
4) Tool tracking layers;
5) Build CPSS layer stack and bond;
6) Final machining and inspection.

In this process, the Kevlar honeycomb layers will act as spacers and stiffeners of the structure. The honeycomb and the resin impregnated Kevlar are extremely pliable until bonded and cured, and each layer must be placed into the right doubly curved shape thanks to the use of a mold structure.

3) Demonstrator Manufacturing

Based on the trade-off criteria listed in Section III.B, it was decided to adopt the approach based on conventional etching techniques on thin dielectric films. In particular, for the manufacturing of the final demonstrator, the following two approaches were considered. With the first approach, the patterned film layers are manufactured in several small parts assembled on the Nomex honeycomb layers. The latter are built out of different separate parts. With the second considered approach, the patterned film layers are

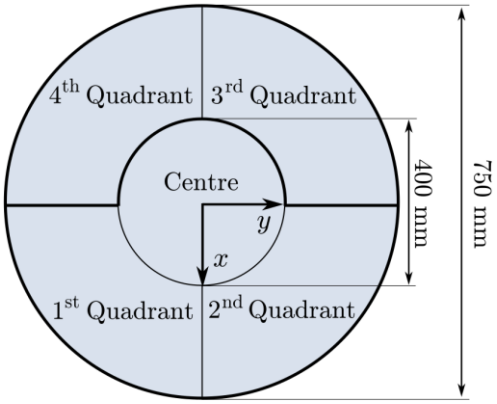

Fig. 13. Subdivision of the demonstrator in different parts to be manufactured separately and assembled in a second phase.

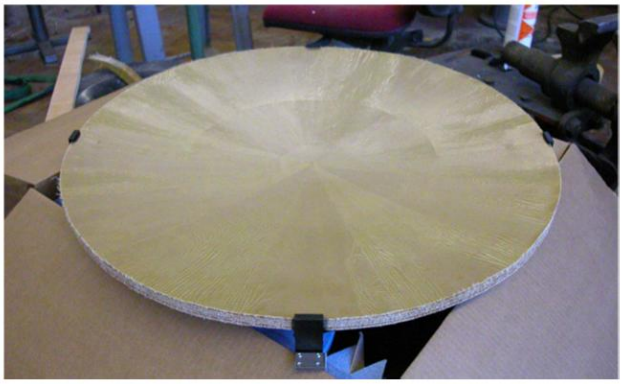

Fig. 14. Doubly curved CPSS demonstrator (diameter D = 75 cm).

manufactured in two parts to be assembled on corresponding Nomex honeycomb layers, built out of maximum two separate parts.

The first option alleviates the problem of the creasing (smaller areas of films have to be applied onto the doubly curved substrate), but, at the same time, it introduces issues of alignment and possible gaps between the different parts. The best option, from this point of view is to manufacture the hard substrates in two pieces, taking into account the maximum workable sizes, and subdivide the patterned films in smaller parts, finding the best compromise in terms of minimum sizes and alignment/assembling issues. On one side, the smaller the parts are, the less critical the creasing problem is; on the other side, the less parts have to be assembled the less problematic the alignment is and the less is also the impact of gaps in the meander lines. The structure that was considered to offer the best compromise in this respect is the one shown in Fig. 13. The hard substrates are divided into two parts, one consisting of 1st and 2nd quadrant plus the center together and a second one consisting of the 3rd and 4th quadrants together. The patterned films instead are divided in the five parts shown in Fig. 13. The central part has been kept as large as possible to avoid the presence of gaps in the part of the CPSS where the EM fields are more intense.

In the second option, the hard substrates consist of one unique piece, while the patterned films are built in two pieces: one consisting of 1st and 2nd quadrant plus the centre together and a second one consisting of the 3rd and 4th quadrants together. These two halves are joint together during the bonding stage of the complete structure. This approach makes the overall manufacturing process less complicated, reduces the problem of gaps and ensures the best alignment between different parts. At the same time, the problem of creasing is expected to be more severe since larger areas of film are applied to the doubly curved substrate.

Some experiments brought to the conclusion that the second option resulted in less manufacturing complexity considering that enough confidence was achieved on the capability of controlling the creasing problem. The fabricated doubly curved CPSS reflector is shown in Fig. 14, where the segmentation contour can be seen in the hardware.

4) Demonstrator Testing Results

The fabricated LH-CPSS demonstrator was characterized experimentally at the near-field range of the Dutch organization for applied scientific research (TNO). The antenna range is suitable for antenna characterization at 0.5-75 GHz, and for the specific measurement campaign an Agilent N5242A PNA-X network analyzer was used. The demonstrator was illuminated by a linearly polarized Narda standard gain horn, which was located with its phase center at the focal point of the demonstrator in a center fed configuration, providing an illumination taper of -10 dB at the edges of the reflector. The feed antenna was simulated in TICRA Tools and the results showed good agreement with experimental results in both co- and cross-polar patterns. The ratio of the co-polarized and the cross-polarized scattering components was higher than 30 dB over the beam area that illuminates the reflectors.

The reflection and transmission properties of the demonstrator were evaluated through a planar scan using an open-ended waveguide antenna. In the transmission case the scanning plane was located at the backside of the DUT, and in the reflection case the scanning plane was located at the same side of the DUT as the feed antenna. The experimental setup used in the reflection and transmission measurements are presented in Fig. 15. The acquired field data is expressed in θ, ϕ coordinates in the angular range θ = [-5,5]° and ϕ = [-90,90]°, with 125 measurement points in θ and ϕ, respectively. Measurements were taken at 16 frequency points in the range [10.75,14.5] GHz with the increment 0.25 GHz between each point.

In the same manner as in the characterization of the planar demonstrator in Section III.A, the scattering in CP of the doubly curved demonstrator was evaluated by measuring the orientation combinations *HH,VV,VH,HV* between the feed antenna and the scanning antenna. The two antennas had to be manually rotated in between each subsequent measurement. Similar reference measurement cases were used for the doubly curved demonstrator as those introduced in Section III.A, *i.e.* empty setup measurements in transmission, and in reflection a metal reflector of the same size as the LH-CPSS was measured. Simulated and measured patterns of the reference metallic reflector were compared to validate the measurement setup. Good agreement was

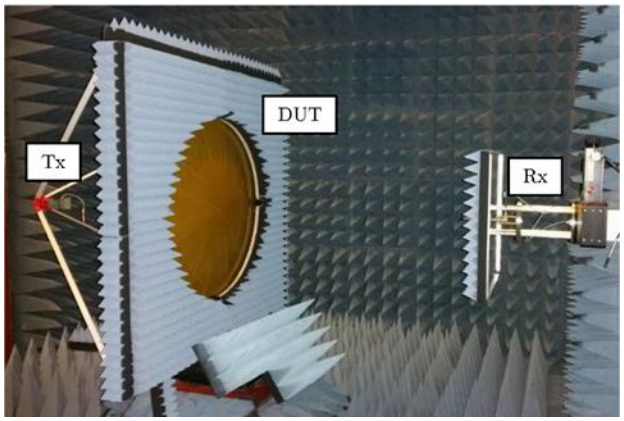

(a)

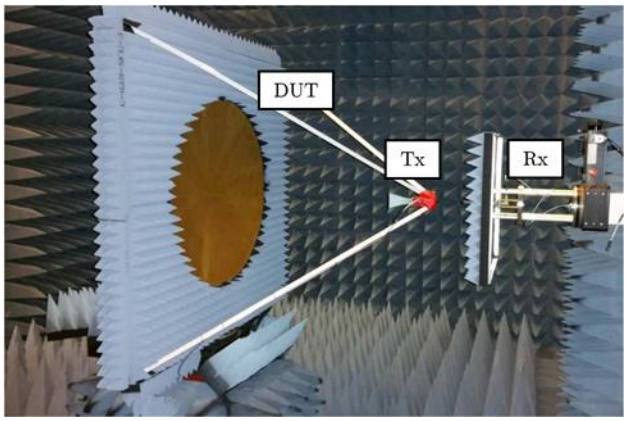

(b)

Fig. 15. LH-CPSS reflector in transmission setup (a) and reflection setup (b).

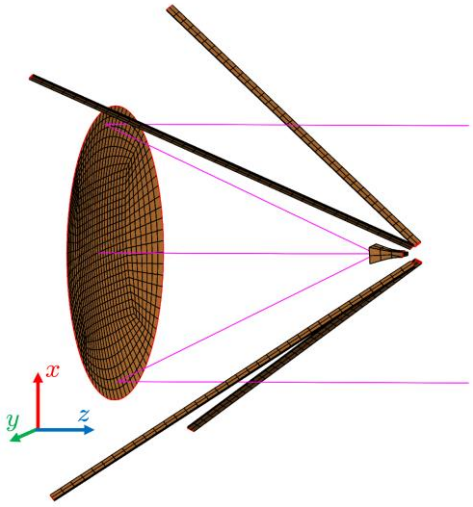

Fig. 16. Simulation model of center fed LH-CPSS reflector with f = 75 cm (f/D = 1) to be compared with the fabricated demonstrator.

observed both for co- and cross-polar lobes, thus indicating a desirable accuracy of the experimental setup.

To evaluate the performance of the LH-CPSS demonstrator, a simulation model of the feed horn, supporting struts and the LH-CPSS demonstrator was implemented in TICRA Tools as in Fig. 16. The LH-CPSS was simulated by importing the scattering properties of the planar CPSS design

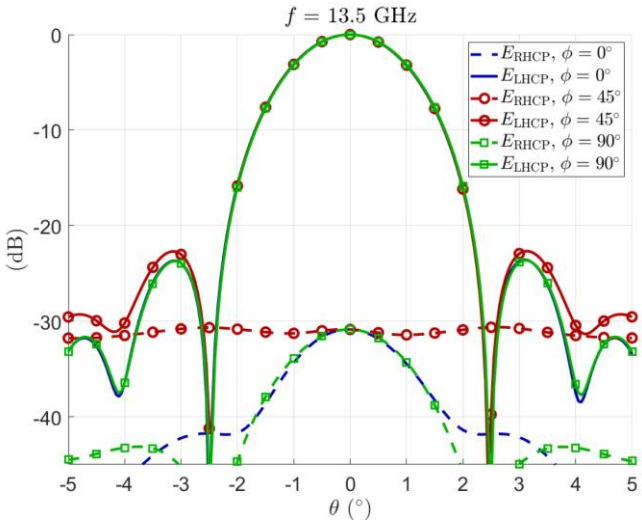

Fig. 17. Simulation results of the CPSS reflector in Fig. 16 at 13.5 GHz. The reflector is illuminated in LHCP at 13.5 GHz and the reflected pattern is determined in LHCP and RHCP, respectively.

in Section II.A as a .tep file, in the same manner as in Section II.B. First, the feed pattern was analyzed using a CAD model of the horn which was simulated using the TICRA ESTEAM method of moments (MoM) solver, then the scattering from the LH-CPSS, illuminated by the feed horn, was simulated using the PO solver in GRASP. Finally, the blockage of the struts and the feed horn was calculated using MoM, and the total scattering of the structure was calculated as the sum of all the mentioned scattering components.

The reflected patterns of the simulated LH-CPSS were evaluated in CP for RHCP and LHCP illumination. The simulated CP illumination cases were achieved by illuminating the LH-CPSS with the feed horn in horizontal and vertical orientation and adding the scattering components in phase quadrature. Simulation results at 13.5 GHz are presented in Fig. 17 for LHCP illumination. Here it can be seen that some cross-polar scattering is present, although at a relatively low level of about 31 dB below the co-polar peak value. In the case of RHCP illumination, the RHCP reflection was 20 dB below the co-polar peak value for LHCP illumination, and the corresponding cross-polar LHCP reflection was about 31 dB below the LHCP co-polar peak. A similar performance was observed of the simulated LH-CPSS at other discrete frequencies throughout the range 10.75-14.50 GHz. Furthermore, the corresponding simulation case of the setup in Fig. 16, but with the realistic CPSS model replaced with an ideal LH-CPSS, resulted in an on-axis XPD of about 45 dB for LHCP illumination. The corresponding value for RHCP illumination was higher than 45 dB.

We now turn to the measured patterns for the CPSS reflector. The measured radiation patterns in CP at 13.5 GHz are shown in Fig. 18, where the top plot shows the reflected pattern in CP for horizontal LP illumination, and in the bottom plot the pattern in CP for vertical LP illumination is presented. It is seen that the measured cross-polarization in Fig. 18 for LP illumination is higher than predicted for CP illumination in the simulation in Fig. 17. It is also noted that the cross-polarization levels are slightly higher for the vertical illumination than for the horizontal illumination. The LH-

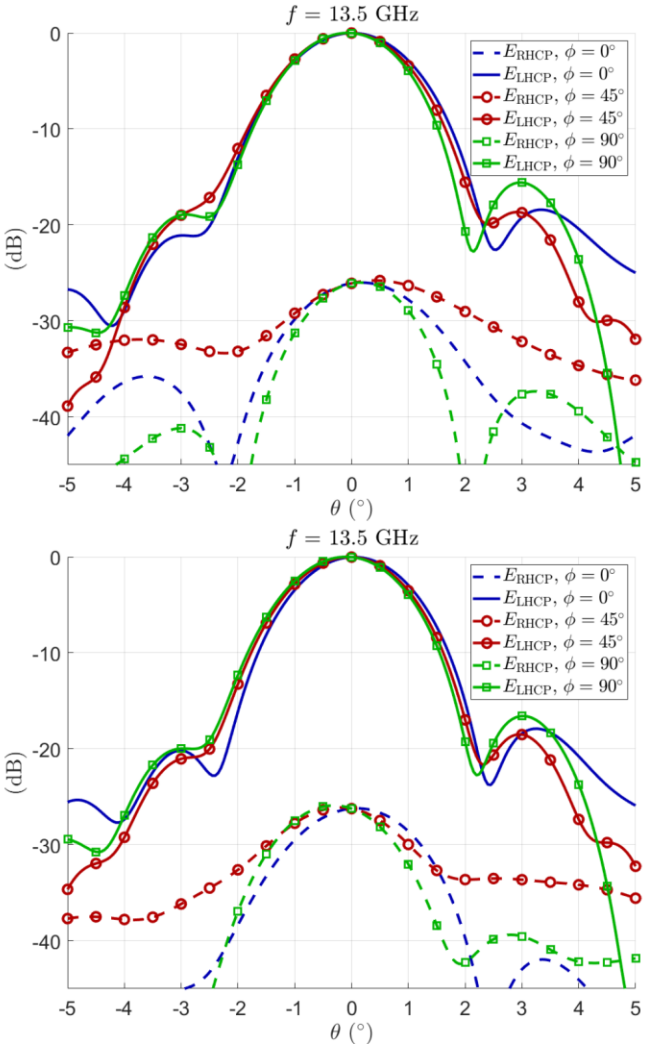

Fig. 18. Experimental results of the fabricated CPSS reflector. The reflector is illuminated at 13.5 GHz with horizontal LP (top) and with vertical LP (bottom) and the reflected pattern is determined in LHCP and RHCP, respectively.

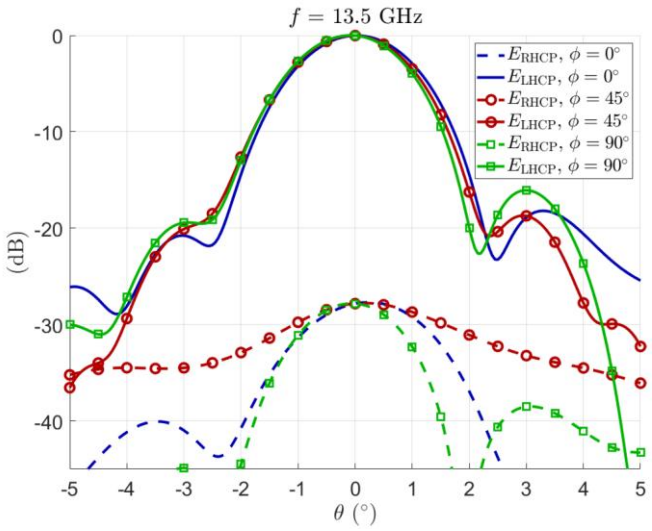

Fig. 19. Experimental results of the fabricated CPSS reflector. The reflector is illuminated in LHCP at 13.5 GHz and the reflected pattern is determined in LHCP and RHCP, respectively.

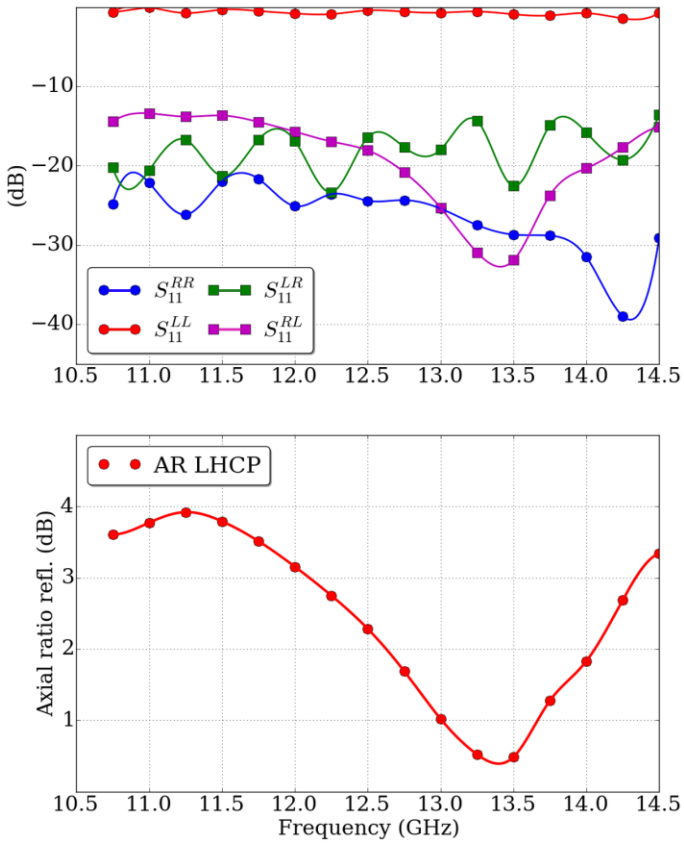

Fig. 20. Experimental results of the fabricated LH-CPSS reflector. The normalized far-field scattering parameters in reflection are presented at the top and the AR of the reflected signals are presented at the bottom for incident LHCP.

CPSS has a wider co-polar pattern shape, with increased sidelobe levels compared to the simulated results in Fig. 17.

The results in Fig. 18 for horizontal and vertical polarization illumination of the doubly curved demonstrator were added in phase quadrature in post-processing to form the CP reflection antenna patterns for RHCP and LHCP illumination. In this step, it was found that a phase drift was present in the reference scattering data when the Tx antenna was placed in vertical orientation in relation to the horizontal orientation case. This effect was numerically compensated for in order to extract the normalized scattering data for LHCP and RHCP illumination of the demonstrator. In Fig. 19 the antenna patterns in CP for LHCP illumination of the demonstrator are presented.

The XPD of the measured results is in acceptable agreement with the simulated results in Fig. 17, where the measured on-axis XPD is about 3 dB higher than in the simulations. The biggest difference is noted in terms of the high sidelobes in the demonstrator results. In the case of RHCP illumination, the experimental results were in the same order of magnitude as in the simulations, with reflection levels at about 20 dB below the co-polarized peak value for LHCP illumination. The co-polarized LHCP scattering of the fabricated LH-CPSS was compared to that of the metallic reference reflector to evaluate the reflection loss of the demonstrator. The relative reflection loss of the demonstrator

was found to be 0.7 dB at 10.75 GHz, 0.9 dB at 13.5 GHz, and 0.7 dB at 14.5 GHz.

The far-field scattering parameters and the AR of waves reflected by the doubly curved LH-CPSS were measured as a function of frequency in the on-axis direction. The scattering parameters were evaluated using the above-mentioned normalization with the solid reference reflector. The results are presented in Fig. 20 as markers at 16 frequency points in the range [10.75,14.50] GHz, and the curves correspond to a cubic interpolation of the experimental data. The results indicate that the co-polar reflection of LHCP waves is high, and the co-polar reflection of RHCP waves is low, which is a desirable behavior. The on-axis co-polarized LHCP reflection coefficient of the doubly curved LH-CPSS demonstrator is in the order of 0.5-1.5. dB over the frequency band 10.75-14.5 GHz. This result can be compared with the fabricated planar CPSS demonstrator results in Fig. 12 where a reflection loss of less than 0.5 dB over the same frequency band is observed. The LHCP AR bandwidth in Fig. 20 is significantly less than that of the planar CPSS design in Section III.A. This indicates that the CP selectivity of the doubly curved CPSS is not as pure as for the planar demonstrator in Section III.A. However, it can also be seen that acceptable LHCP AR levels are achieved in the frequency range of about 12.7-13.9 GHz in relation to the relaxed AR requirement put forward in Section II.B. It is noted that the two cross-polarization scattering components in Fig. 20 are not equal, which is caused by the losses in the structure as well as the fact that it is the far-field scattering parameters of the antenna system that are evaluated. When the CPSS demonstrator is illuminated with an RHCP wave, the main reflection contribution is in LHCP, which is seen in Fig. 20.

In order to identify potential fabrication errors, the demonstrator was inspected visually, and the thicknesses of the reflector layers were measured. Excess portions of the doubly curved demonstrator that were made available after the reflector was trimmed to size were inspected. It was found that the thicknesses of the inner and outer honeycomb spacers were 2.9 mm and 5.0 mm. These values should be respectively 2.6 mm and 4.9 mm as can be seen in Table II. This deviation is acceptable and should not result in the degradation in bandwidth that can be seen in Fig. 20. The overall thickness of the CPSS reflector was measured at 6 different points across the surface and it was shown to be in the range of 16.6-17.0 mm, to be compared to the expected thickness of 16.0 mm.

Effects of delamination were not detected in the inspection. It was observed that considerable wrinkling occurred in the printed layers, mostly in the outer regions of the reflector. The inner circle, which is the portion of the reflector that will receive most of the feed power, was relatively less affected by the wrinkling. It is safe to mention that with the current manufacturing process wrinkling is an inevitable side effect, that might potentially have a significant impact on the scattering properties of the demonstrator. The magnitude of the effect of wrinkling on the scattering properties of the reflector is difficult to evaluate through simulations. However, a sensitivity analysis was carried out of the CPSS on unit cell level where translations and rotations of each printed layer were introduced. The results indicated that misalignments due to relative pattern translations have a very minor effect on the performance of the structure, but misalignment due to unwanted rotations of the subsequent layers has a more significant effect on the performance. It is anticipated that the curvature of the structure will imply mainly translational misalignments of the cascaded layers.

It should also be stated that it was not possible to completely assess whether wrinkling and delamination had occurred at the center of the different regions of the reflector without a destructive inspection approach. Another aspect that might affect the scattering properties of the demonstrator is the joint between the two parts of the reflector. This joint will impact the electrical properties of the printed layers since the copper patterns consist of continuous meander line strips. Furthermore, if some of the printed layers were not aligned with respect to the other layers of the same panel, or if the printed layers of the separate panels were not aligned with respect to one another, this would potentially have resulted in significant performance degradation of the demonstrator.

The fact that the feed horn and the receiving antenna had to be manually rotated may introduce phase variations in the subsequent measurements used to compute the scattering response in CP. Phase errors caused by manual antenna rotations were assessed and were shown to only lead to marginal errors. In conclusion, it was not possible to fully judge whether the differences between the experimental results and simulations are due to fabrication errors in the demonstrator or to errors associated with the experimental setup that was used. From the discussions above, it is reasonable to assume that the bandwidth degradation of the CPSS demonstrator was mainly due to inaccuracies and limitations associated with the fabrication process of the doubly curved multilayered structure.

These results indicate that with the current state of manufacturing processes for large structures, the considered stack-up of multiple printed layers is still a challenge to implement in a doubly curved configuration. The antenna configuration described in [30] with the CPSS as sub-reflector is currently a preferred geometry. However, this would require more complex feed systems for the shaped contoured beams investigated in this paper, similar to the ones reported in [11], [12] in the case of an LP antenna system.

IV. Conclusion

A reflector antenna system in Ku-band has been presented corresponding to a circular polarization equivalent of the linear polarization dual-gridded reflector. The system is based on a wideband, non-resonant circular polarization selective surface (CPSS) consisting of multiple layers of printed meander lines. The CPSS was initially designed as a planar surface and later implemented as a doubly curved reflector. This concept was simulated as a contoured-beam reflector satellite antenna system, consisting of two shaped doubly curved CPSS reflectors.

A planar CPSS demonstrator was fabricated and tested experimentally, and good agreement with simulations was observed. Different fabrication methods were evaluated for manufacturing a doubly curved CPSS demonstrator, and the most mature concept was implemented. The doubly curved

demonstrator did not provide as good performance as in corresponding simulations in terms of bandwidth. Unfortunately, the costs associated with the fabrication and testing of a new hardware prototype made it difficult to move ahead with a new prototype. However, the demonstrator shows performances that, although not compliant with the requirements, are acceptable given the degrees of difficulty for this first time doubly curved multilayer demonstrator.

It is concluded that the manufacturing approach adopted is not ideal for a multilayer doubly curved structure. It would be preferable to adopt techniques that allow depositing the metallic patterns directly on top of a curved surface. Further investigations of this type of techniques can potentially result in significant improvements with respect to reduced fabrication complexity and improved fabrication accuracy.

ACKNOWLEDGEMENT

The authors of this paper would like to thank Printech Circuit Laboratories Ltd., Chelmsford, U.K., for the manufacturing of the flat breadboard sample and the curved demonstrator. We thank Elena Saenz, European Space Agency (ESA), Noordwijk, The Netherlands, for the measurement of the flat breadboard, and Roland Bolt, TNO, Delft, The Netherlands, for the support in the development and measurement of the curved circular polarization selective surface (CPSS) demonstrator and the very useful discussions on the results analysis.

REFERENCES

[1] W. A. Imbriale, S. S. Gao, and L. Boccia, Eds., *Space Antenna Handbook.* Hoboken, NJ, USA: Wiley, 2012.

[2] S. Rao, L. Shafai, and S. K. Sharma, Eds., *Handbook of Reflector Antennas and Feed Systems*:*Applications of Reflectors, vol. 3*. Norwood, MA, USA: Artech House, 2013.

[3] W. Chang, E. Dudok, N. Nathrath, E. Sommer and G. Crone, "Communication antenna subsystem for the Chinese satellite DFH-3," in *Proc. 19th European Microw. Conf.*, 1989, pp. 699–705.

[4] E. Dudok, N. Nathrath, E. Sommer, H. Wolf and G. Crone, "Development of a multi-shaped beam antenna in C-band," in *Proc. 19th European Microw. Conf.*, 1989, pp. 1110–1117.

[5] W.J. Hall, *et al.*, "Satellite antenna subsystem using shaped reflector and multiple feed gridded reflectors," in *Proc. 6th Int. Conf. Antennas and Propag., ICAP89*, 1989, pp. 60-64.

[6] T.R. Waterfield, R.J. Wimmer and D.P.S. Malik, "The use of shaped dual-shell gridded reflectors in multi-beam and shaped-beam satellite antennas," *IEE Colloquium on Reflector Antennas*, 1992, pp. 8/1-8/7.

[7] S. Sierra-Garcia, *et al.*, "W3A top floor antenna," in *Proc. 10th Int. Symp. Antennas Techno. Applied Electromagnetics (ANTEM)*, 2004, pp. 1–3.

[8] L. Martins Camelo, "The Express AM4 top-floor steerable antennas," in *Proc. 14th Int. Symp. Antennas Techno. Applied Electromagnetics (ANTEM)*, 2010, pp. 1–4.

[9] H. Ohmine, Y. Kobayashi, "High performance reflectors for telecom space antennas in MELCO," in *Proc. 6th European Conf. Antennas Propag., (EuCAP)*, 2011, pp. 3331-3335.

[10] F.A. Regier, "The ACTS multibeam antenna," *IEEE Trans. Microw. Theory and Technique*, vol. 40, no. 6, Jun. 1992, pp. 1159–1164.

[11] Y. Cailloce, *et. al.*, "Ku-multibeam antenna with polarisation grids", in *Proc. IEEE Int. Symp. AP-S*, Honolulu, Jun. 2007, pp. 5183–5186.

[12] E. Vourch, *et al.*, "Satellite accommodation of a Ku multibeam antenna with polarisation grid sub-reflector", in *Proc. Int. Symp. Antennas Propag., ISAP*, Niigata, Aug. 2007, pp. 1298-1301.

[13] M. Albani, *et al.*, "Concepts for polarising sheets & 'dual-gridded' reflectors for circular polarisation", *Special COST ASSIST session, ICECom*, Dubrovnik, Sep. 2010, pp. 1–4.

[14] R. Pierrot, "Reflector for circularly polarized waves," Mar. 30 1970, US Patent 3,500,420, (French Patent No. 89 609, 1 512 598, Dec. 30, 1966).

[15] W.V. Tilston, T. Tralman, and S.M. Khanna, "A polarization selective surface for circular polarization," in *Proc. Antennas Propag. Society Int. Symp.*, 1988, pp. 762–765 vol.2.

[16] G.A. Morin, "A simple circular polarization selective surface (CPSS)," in *Proc. Antennas Propag. Society Int. Symp.*, *Merging Technologies for the 90's*, 1990, pp. 100–103 vol.1.

[17] W. Tang, *et al.*, "Study of coupled split-ring resonator arrays for circular polarization selective surfaces," in *Proc. IEEE Int. Symp. Antennas Propag., USNC/URSI Nat. Radio Sci. Meeting*, Jul. 2015, pp. 362–363

[18] W. Tang, *et al.*, "Coupled split-ring resonator circular polarization selective surfaces," *IEEE Trans. Antennas Propag.*, vol. 65, no. 9, pp. 4664–4675, Sept. 2017.

[19] M.-A. Joyal and J.-J. Laurin, "A cascaded circular-polarization-selective surface at K band," in Antennas and Propagation (APSURSI), 2011 IEEE International Symposium on. IEEE, 2011, pp. 2657–2660.

[20] M. Joyal and J. Laurin, "Analysis and design of thin circular polarizers based on meander lines," *IEEE Trans. Antennas Propag.*, vol. 60, no. 6, pp. 3007–3011, 2012.

[21] S. Momeni, H. Abadi and N.Behdad, "A broadband circular polarization selective surface," *Journal of Applied Physics*, vol. 119, no. 244901, 2016.

[22] D. Sjöberg and A. Ericsson, "A multi layer meander line circular polarization selective structure (MLML-CPSS)," in *Proc. 8th Eur. Conf. Antennas Propag. (EuCAP*), 2014, pp. 464–468.

[23] A. Ericsson and D. Sjöberg, "A performance study of circular polarization selective structures," in *Proc. 9th Eur. Conf. Antennas and Propag. (EuCAP).*2015, pp. 1–5.

[24] C. Cappellin, *et al.*, "Design and analysis of a reflector antenna system based on doubly curved Circular Polarization Selective Surfaces," in *Proc. 10th Eur. Conf. Antennas Propag.* (EuCAP), 2016, pp. 1–5.

[25] A. Ericsson and D. Sjöberg, "Design and Analysis of a Multilayer Meander Line Circular Polarization Selective Structure," *IEEE Trans. Antennas and Propag.*, vol. 65, no. 8, pp. 4089–4101, Aug. 2017.

[26] A. Ericsson, J. Lundgren and D. Sjöberg, "Experimental Characterization of Circular Polarization Selective Structures Using Linearly Single-Polarized Antennas," *IEEE Trans. Antennas and Propag.*, vol. 65, no. 8, pp. 4239–4249, Aug. 2017.

[27] J. Lundgren, A. Ericsson and D. Sjöberg, "Design, Optimization and Verification of a Dual Band Circular Polarization Selective Structure," in *IEEE Trans. Antennas and Propag.*, vol. 66, no. 11, pp. 6023–6032, Nov. 2018.

[28] A. Hessel, M. H. Chen, R. C. M. Li, and A. A. Oliner, "Propagation in periodically loaded waveguides with higher symmetries," *Proc. IEEE*,

[29] vol. 61, no. 2, pp. 183–195, Feb. 1973.J.E. Hansen (Ed.), *Spherical Near-Field Antenna Measurements*, Peter Peregrinus Ltd., London, United Kingdom, 1988.

[30] N. J. G. Fonseca and C. Mangenot, "High-performance electrically thin dual-band polarizing reflective surface for broadband satellite applications," *IEEE Trans. Antennas Propag.*, vol. 64, no. 2, pp. 640–649, Feb. 2016.

Andreas Ericsson (M'13) received the M.Sc. degree in engineering physics and the Ph.D. degree in electrical engineering from Lund University, Lund, Sweden, in 2013 and 2017, respectively. He joined TICRA in Denmark in 2018 where he is currently the Product Lead for Antenna Measurement Software products.

He is currently involved in multiple ESA activities on design and analysis of reflectarray antennas and frequency selective surfaces for satellite communication applications, as well as source reconstruction for antenna diagnostics. His research interests include antenna measurement techniques, electromagnetic scattering, and design and analysis of frequency and polarization selective surfaces. Dr. Ericsson was a recipient of the Student Paper Award at URSI GASS 2014 in Beijing.

Daniel Sjöberg (M'13–SM'20) received the M.Sc. degree in engineering physics and the Ph.D. degree in electromagnetic theory from Lund University, Lund, Sweden, in 1996 and 2001, respectively.

In 2001, he joined the Electromagnetic Theory Group, Lund University, where he became a Docent in electromagnetic theory, in 2005. He is currently a Professor and the Head of the Department of Electrical and Information Technology, Lund University. His research interests are in electromagnetic properties of materials, composite materials, homogenization, periodic structures, numerical methods, radar cross section, wave propagation in complex and nonlinear media, and inverse scattering problems.

Giampiero Gerini (M'92–SM'08) received the M.Sc. degree (summa cum laude) and the Ph.D. degree in electronic engineering from the University of Ancona, Italy, in 1988 and 1992, respectively.

From 1992 to 1994 he was Assistant Professor of Electromagnetic Fields at the same University. From 1994 to 1997, he was Research Fellow at the European Space Research and Technology Centre (ESA-ESTEC), Noordwijk, The Netherlands, where he joined the Radio Frequency System Division. Since 1997, he has been with the Netherlands Organization for Applied Scientific Research (TNO), The Hague, The Netherlands. At TNO Defence Security and Safety, from 1997 to 2013, he was Chief Senior Scientist of the Antenna Unit in the Radar Technology Department. In 2014, he has joined the Optics Department where he is charge of the metamaterial research program. In 2007, he has been appointed as full Professor in the Faculty of Electrical Engineering of the Eindhoven University of Technology, The Netherlands, with a chair on "Novel Structures and Concepts for Advanced Antennas". Since 2017, he has a new chair on "Material Engineering from Microwaves to Optics".

He was co-recipient of the 2008 H. A. Wheeler Applications Prize Paper Award of the IEEE Antennas and Propagation Society. He was co-recipient also of the Best Innovative Paper Prize of the 30th ESA Antenna Workshop in 2008 and of the best antenna theory paper prize of the European Conference on Antennas and Propagation (EuCAP) in 2010. His main research interests are phased arrays antennas, electromagnetic bandgap structures, frequency selective surfaces, metamaterials and metasurfaces (from microwaves up to optical frequencies). The main application fields of interest are imaging, metrology, sensing, radar and telecommunication systems.

Cecilia Cappellin (M'08) is Head of the Applied Electromagnetics team and Product Lead for Reflector Systems Designs at TICRA in Denmark. She joined TICRA in 2004 and has now more than 15 years of experience in electromagnetic modelling of reflector antennas. She is currently deeply involved in the ESA/EU activities on large mesh reflectors and in the ESA studies on advanced multi-beam radiometers for future ocean observations. As a member of the AEM team she actively participates in the test and development cycle of all TICRA software products and assists TICRA's customers under their technical support contract. Cecilia received her MSc degree from the University of Siena (Italy) in 2004 and her Industrial PhD degree from the Technical University of Denmark in 2007.

Frank Jensen (S'69–M'72) is an Emeritus employee at TICRA in Copenhagen. He has worked with evaluation of antenna measurements, especially compact test range performances, he has designed and constructed high precision dual-polarized near-field probes, and he has developed electromagnetic modelling approaches to predict performances of low gain antennas on large satellites. In his PhD thesis he developed the basis for the spherical near-field to far-field transformation with full probe correction. He has been a senior member of AMTA since 2008 and received the AMTA Distinguished Achievement Award 2013.

Peter Balling is a retired expert in the field of satellite antenna design, analysis and testing. For 28 years he was the managing director of Antenna System Consulting (ASC), Taastrup, Denmark. His main expertise is in design, analysis and testing of multibeam, contoured-beam and reconfigurable antennas, including reflector and array antennas, feed systems, passive and active beamforming networks as well as single-feed-per-beam offset-reflector scan-degradation compensating systems.

Nelson J. G. Fonseca (M'06–SM'09) received the M.Eng. degree from Ecole Nationale Supérieure d'Electrotechnique, Electronique, Informatique, Hydraulique et Télécommunications (ENSEEIHT), Toulouse, France, in 2003, the M.Sc. degree from the Ecole Polytechnique de Montreal, Quebec, Canada, also in 2003, and the PhD degree from Institut National Polytechnique de Toulouse – Université de Toulouse, France, in 2010, all in electrical engineering.

Since 2009, he works in the Antenna and Sub-Millimetre Wave Section, European Space Agency (ESA), Noordwijk, The Netherlands. His current research interests include multiple beam antennas for space missions, beam-former theory and design, as well as user terminal antennas.

Dr. Fonseca is serving as Associate Editor for the *IET Microwave, Antennas and Propagation (MAP) journal* and for the *IEEE Transactions on Microwave Theory and Techniques (TMTT).* He is also serving as Editorial Board member for the upcoming *IEEE Journal of Microwaves (JMW)*. He is a board member of the European School of Antennas (ESoA) since January 2019 and coordinator of the ESA/ESoA course on *Antennas for Space Applications* for which he was voted best lecturer by the participants of the 2020 edition. He received several prizes and awards, including the Best Young Engineer Paper Award at the 29th ESA Workshop on Antennas in 2007 as well as multiple ESA Technical Improvement Awards.

Peter de Maagt (S'88–M'88–SM'02–F'08) was born in Pauluspolder, The Netherlands, in 1964. He received the M.Sc. and Ph.D. degrees in electrical engineering from Eindhoven University of Technology, Eindhoven, The Netherlands, in 1988 and 1992, respectively.

From 1992 to 1993, he was a Station Manager and Scientist with an INTELSAT propagation project in Surabaya, Indonesia. Currently, he is with the European Space Research and Technology Centre (ESTEC), European Space Agency (ESA), Noordwijk, The Netherlands. He spent the summer of 2010 as a Visiting Research Scientist at Stellenbosch University, Stellenbosch, South Africa. His research interests include the areas of millimeter and submillimeter-wave reflector and planar integrated antennas, quasi-optics, electromagnetic bandgap antennas, and millimeter- and submillimeter-wave components.

Dr. de Maagt served as an Associate Editor for the IEEE Transactions on Antennas and Propagation from 2004 to 2010, and was the Co-Guest Editor of the November 2007 Special Issue on Optical and Terahertz Antenna Technology. He was the co-recipient of the H. A. Wheeler Award of the IEEE Antennas and Propagation Society for the Best Applications Paper of 2001 and 2008. He was granted an ESA Award for Innovation in 2002, and an ESA award for Corporate Team Achievements for the Herschel and Planck Program in 2010. He was the co-recipient of Best Paper Awards at the 2006 Loughborough Antennas Propagation Conference (LAPC) and 2007 the International Workshop on Antenna Technology (IWAT).